Acta Cryst. (1969). B25, 1156

Multiple Phase Formation in the Binary System Nb_2O_5–WO_3. VI. Electron Microscopic Observation and Evaluation of Non-Periodic Shear Structures

BY J. G. ALLPRESS AND J. V. SANDERS
Division of Tribophysics, CSIRO, Melbourne, Australia

AND A. D. WADSLEY*
Division of Mineral Chemistry, CSIRO, Melbourne, Australia

(*Received* 11 *June* 1968)

High-temperature Nb_2O_5 and a number of mixed Nb/W oxides with ordered shear structures have been examined by electron microscopy and electron diffraction. The generation of lattice images from the direct beam and one or more of the diffracted beams, *hkl*, affords a powerful method of studying inhomogeneities within their structures. The faults, which are planar, correspond in any one compound to regions of a second phase intergrown with it, and may be as small as half a unit cell in width – a single fault, or a larger group representing a domain. The composition of these non-periodic regions differs from that of the host, and their presence will give rise to a composition range for the phase in which they occur.

Introduction

Niobium pentoxide forms extensive series of compounds with WO_3. A partial phase diagram together with the crystal structure determination of a group of four of these were reported in parts I–IV of the above running title (Roth & Wadsley, 1965*a*,*b*,*c*,*d*) while a fifth, found originally by Gruehn (1965) was examined in part V (Andersson, Mumme & Wadsley, 1966).

The first four compounds $WNb_{12}O_{33}$, $W_3Nb_{14}O_{44}$, $W_5Nb_{16}O_{55}$ and $W_8Nb_{18}O_{69}$ are related among themselves by a common structural principle. Each one contains blocks of metal–oxygen octahedra joined as in the rhenium trioxide structure by sharing corners and extending indefinitely in the third direction. The structures of these phases are identical except for the size of the block, which in cross-section consists of three octahedra by four for $WNb_{12}O_{33}$, 4×4 for $W_3Nb_{14}O_{44}$, 4×5 for $W_5Nb_{16}O_{55}$ and 5×5 in the case of $W_8Nb_{18}O_{69}$ [Fig. 1(*a*)–(*d*)].

The fifth phase $W_4Nb_{26}O_{77}$, described in part V, differs somewhat from the other four. Its structure contains parallel segments of $WNb_{12}O_{33}$ and $W_3Nb_{14}O_{44}$, infinite in two directions and alternating in a regular sequence in the third, and is, therefore, an intergrowth or hybrid of the two phases adjoining it in composition on either side [Fig. 1(*e*)]. Additional examples of these intergrowth phases are reported amongst a group of reduced non-integral-valency niobium oxides (Gruehn & Norin, 1967) and in the niobium oxyfluorides (Andersson, 1965; Gruehn, 1967) where these same or similar structural principles apply.

In all of these compounds individual blocks join by sharing octahedral edges rather than corners, and these regions of higher-than-average density may be referred to as *shear planes* (Wadsley, 1964) criss-crossing the structure at regular intervals. These planes also contain tetrahedrally coordinated metal atoms situated in the channels at the corners of the blocks.

The X-ray structure determination for these five mixed-oxide phases led to an ideal formula for each one of them which was based upon the contents of the unit cell (Roth, Wadsley & Gatehouse, 1964). These formulae represent the chemical composition as determined from phase equilibrium studies (Roth & Wadsley, 1965*a*; Roth & Waring, 1966), but there is some chemical evidence that many of these dual-valency or mixed-oxide niobium phases may have very small but reproducible regions of homogeneity, with the ideal composition representing one of the limits (Gruehn & Schäfer, 1965). The way in which this non-stoichiometry is accommodated within the crystals has not been resolved by X-ray diffraction techniques, because these provide only statistically averaged structures, with details of compositional and crystalline imperfections obscured.

We have, therefore, tackled this problem with electron diffraction and microscopy, which are complementary to X-ray techniques with a number of important advantages. Crystals reasonably transparent to electrons are necessarily very thin, and it is possible to obtain single-crystal diffraction patterns from material much too small for single crystal X-ray work. These patterns can be obtained very quickly, and all of the reflexions within a zone are easily recorded. Their positions correspond closely to undistorted sections of the reciprocal lattice, and the dimensions of the unit cell and the probable space group are readily derived from two or more orientations of the crystals. Furthermore it is a straightforward matter to observe lattice images in electron micrographs of individual crystals if, as in

*We regret to record that Dr A. D. Wadsley died suddenly on 6 January 1969.

the present case, the unit cell is large in at least one direction.

Some of these advantages have already been demonstrated by us in a preliminary study of high-temperature niobium pentoxide (H–Nb_2O_5) and the Nb/W mixed-oxide phases (Allpress, Sanders & Wadsley, 1968). Irregularities in the fringe spacings in lattice images of the mixed-oxides were common, and in this paper we analyse them in detail and discuss the results in terms of the random intergrowth between fragments of crystalline phases with an exact atomic fit at their boundaries.

Experimental

The mixed-oxide specimens used in this study were the original ones examined by Roth & Wadsley (1965*a*) supplemented by some prepared in a parallel study at the University of Münster, Westphalia, and kindly made

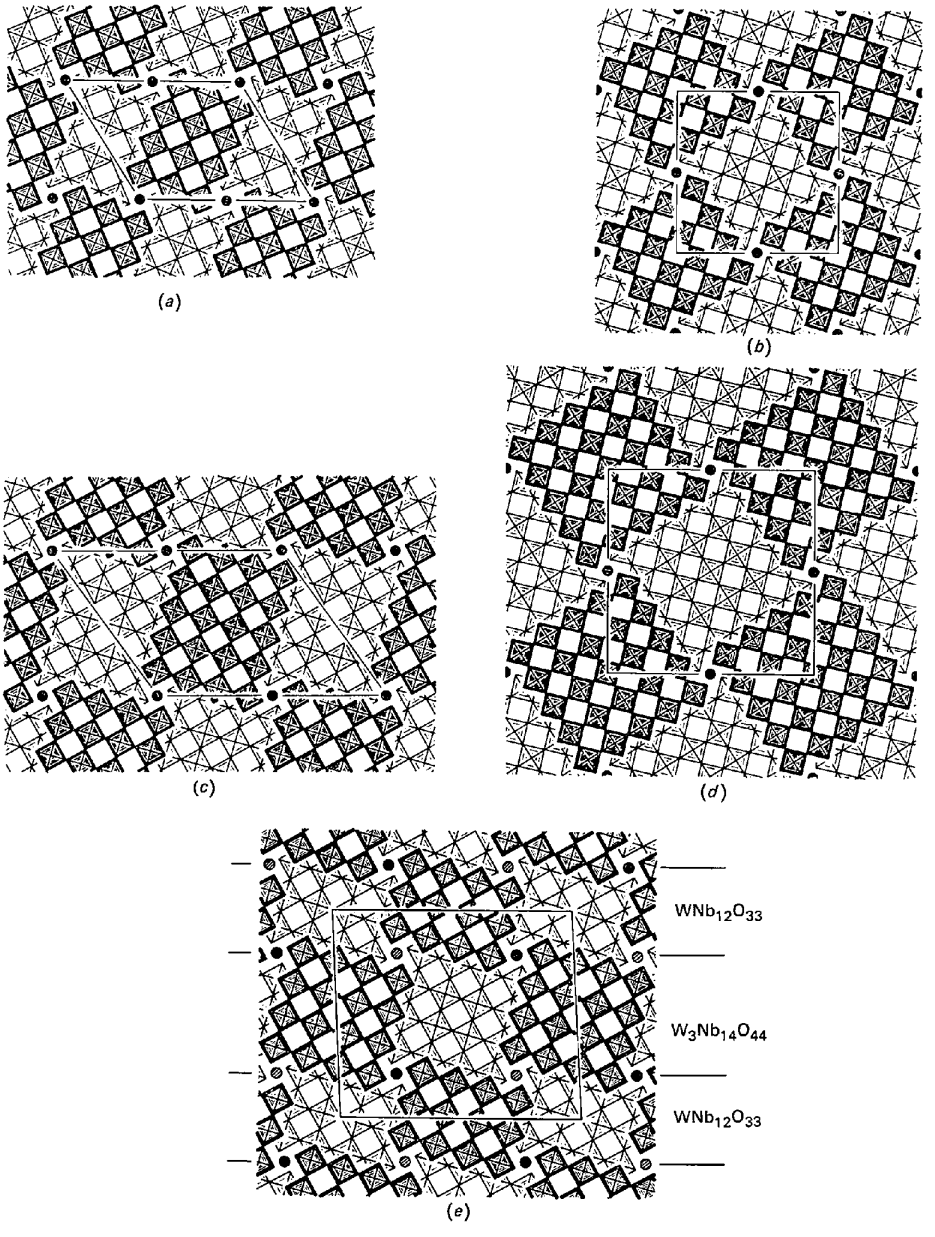

Fig. 1. Idealized sketches of the Nb–W mixed oxides. The squares represent octahedra viewed down their body diagonals, the lighter and darker squares being centred on two parallel planes 1·9 Å apart. The octahedra sharing corners form the structural blocks, and the junctions between light and dark lie in the shear planes, where the octahedra share edges. The circles represent tetrahedrally coordinated metal atoms. (*a*) $WNb_{12}O_{33}$. (*b*) $W_3Nb_{14}O_{44}$. (*c*) $W_5Nb_{16}O_{55}$. (*d*) $W_8Nb_{18}O_{69}$. (*e*) $W_4Nb_{26}O_{77}$, an ordered intergrowth of (*a*) and (*b*).

available by Professor H. Schäfer and Dr R. Gruehn. These were finely ground in an agate mortar, dispersed in methyl chloroform and collected on carbon coated grids. The electron microscope is a Philips' EM200 equipped with a double-tilting stage ($\pm 30°$ in two mutually perpendicular directions) and anticontamination blades cooled to -160 °C. above and below the specimen. Selected area diffraction from crystals reasonably transparent to 100kV electrons showed that the majority were supported with only one long axes normal to the electron beam, but a small proportion of them could be tilted to reveal both long axis. It is necessary to find this unique orientation for each phase where the short axis of symmetry is parallel to the beam, in order to gather the maximum structural information from the specimen.

The primary magnification was usually $\times 150{,}000$. Fringe spacings were estimated from microdensitometer records of the photographic plates with a linear magnification of 50. Their periodicity in unfaulted areas, determined with considerable accuracy by measuring the spacing of up to twenty fringes, was a reliable method of calibrating the magnification, and the non-periodic fringe spacings in faulted areas were measured relative to these with an accuracy of $\pm 10\%$.

Interpretation of fringe patterns in lattice images

Lattice images of crystals of the mixed oxides, consisting of sets of parallel fringes, may be observed when one or more diffracted beams, together with the main electron beam, are passed through the objective aperture in the electron microscope. When this aperture is small (25 microns), the diffracted beams are from crystal planes with spacings between 10 and 20 Å. Their intensities are low because their structure amplitudes are small, and consequently their extinction distance are large. The calculated value for the extinction distance for electrons using the 100 reflexion of H–Nb_2O_5 ($d = 18{\cdot}4$ Å) is $1{\cdot}7 \times 10^4$ Å. Under these conditions the crystals, which are probably about 1000 Å thick, are effectively thin to these diffracted beams, and hence may be considered to be phase gratings (Heidenreich, 1966). This was confirmed experimentally by noting that the contrast of the fringes was weak when the edge of the crystal was in precise focus, but increased as the objective lens was underfocused. The extent of defocus for maximum contrast was greater for larger fringe spacings than for narrow fringes. The amount of defocus, 5000 Å for 20 Å fringes, agrees with that expected for maximum contrast (Heidenreich, 1964). It must be emphasized that this effect does not extend to higher order reflexions with smaller extinction distances. Dark field images from these reflexions exhibited fringes which were clearly dynamical in a crystal whose thickness changed by several extinction distances (Hashimoto, Mannami & Naiki, 1961). Under such conditions the relation between the fringe positions and the contents of the unit cell depends both upon the thickness of the crystal and upon the dynamical diffraction conditions, which are factors not easily determined for many diffracting beams within a crystal. This behaviour is clearly recognizable, and was generally not observed with the lower order reflexions with which we are concerned.

If the crystal behaves as a phase grating, the contrast in the slightly underfocused image represents the projected charge distribution of the crystal (Cowley & Moodie, 1960). Since this property of the image is retained even for non-periodic phase objects, any irregularities which are present in the crystal should also appear. Thus the fringe patterns in the images truly represent the structure of the crystal, with a resolution determined by the restricted number of diffracted beams transmitted through the objective aperture. In our case, these beams came from planes with spacings greater that about 10 Å. The dominant structural features in the mixed oxides having spacings of this order are the shear planes, and they are also regions of higher than average charge density. Hence, we might expect that provided the appropriate reflexions are selected, the shear planes should be resolved in the lattice images, and that anomalies in their spacings should also be revealed.

Structural geometry and representation

The mixed-oxides of niobium and tungsten are readily represented by idealized drawings of their projected structures. Because the projection axis in each case is

Table 1. *Theoretical unit-cell dimensions*

Compound	Symmetry†	Block size	Unit-cell dimensions* (Å) From X-rays a	c	β	Calculated a	c	β
$WNb_{12}O_{33}$	M	4×3	22·37	17·87	123·6°	22·0	17·6	122·7°
$W_3Nb_{14}O_{44}$	T	4×4	21·02			21·0		
$W_5Nb_{16}O_{55}$	M	5×4	29·79	23·08	126·5	29·7	23·2	126·1
$W_8Nb_{18}O_{69}$	T	5×5	26·25			26·6		
$W_4Nb_{26}O_{77}$	M	4×3 / 4×4	29·74	25·97	92·3	29·7	25·8	92·4

* The short axis (b or c for M and T structures respectively) is the same for all compounds $= 3{\cdot}82 \pm 0{\cdot}01$ Å.
† M–side centred monoclinic, T–body centred tetragonal.

short, and corresponds in length to an octahedral body diagonal, these drawings are also cross-sections of the structures and show that the octahedra within each unit cell are centred on two equidistant levels and are joined by edges at the shear planes. Although there are displacements of individual atoms from the ideal positions, the theoretical unit-cell dimensions for a phase can be calculated from its drawing by simple geometry with an accuracy approaching 2% (Table 1), the only assumption being that the length of the octahedral edge is constant at 2·89 Å, the average for all nine independently determined niobate structures (part IV).

A new simple style is now used to illustrate these structures and their associated defects (Fig. 2). The blocks are reduced to rectangles, the heavier and lighter outlines representing the two different levels perpendicular to the projection axes, and the corners of each rectangle are the positions of the corner metal atoms. The tetrahedrally coordinated metal atoms are drawn as circles, and the shear planes are centred about the empty spaces between the blocks. The remaining details are inessential for our purposes and are suppressed by this type of illustration.

Models of the faults found by the electron microscope are proposed on the basis of three criteria. The fringe positions must be consistent with the model, the dimensions of which are calculated in exactly the same way as theoretical unit-cell dimensions. The angular displacement of the fringes running approximately perpendicular to the fault must have both the correct sense and magnitude. This condition is not particularly sensitive unless the fault fringes are grouped together when the displacement, which is always small, can be measured with a protractor. Finally the model, in terms of the sizes and arrangement of octahedral blocks, must be compatible with already known structures.

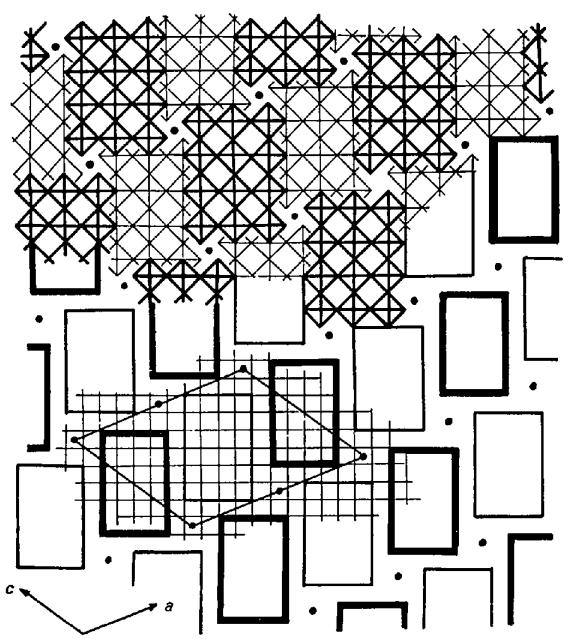

Fig. 2. Idealized sketch of the structure of $WNb_{12}O_{33}$. In the upper part, the octahedra are outlined. In the simpler representation (lower), only the outlines of the blocks of metal atoms are shown. The tetrahedral metal atoms are represented as dots. Part of the square grid on which the drawing is based is also shown.

Results

The relationship between the lattice images and the structures responsible for them is explored for a number of cases shown in Figs. 3, 4, 6, 9, 11 and 12. These examples, taken from a much greater number of micrographs, are typical of the images and of the faults which have been found in these compounds.

H–Nb_2O_5

Fig. 3 illustrates two different lattice images of the same crystal fragment of H–Nb_2O_5 using the direct beam and the 001 and $10\bar{1}$ reflexions respectively. The fringes are remarkably regular, and extend over areas many times larger than the illustration; their periods of 16·8 and 17·7 Å agree well with the spacings d_{100} and $d_{10\bar{1}}$. The absence of dislocations, or indeed of any recognizable defects at this level, is in accord with the severe extinction found during the X-ray structure determination (Gatehouse & Wadsley, 1964). Sub-grains or domains with some variation of fringe spacing noted in a study of niobium (and tantalum) pentoxide films by Spyridelis, Delavignette & Amelinckx (1967) have never been observed by us in H–Nb_2O_5, and we have concluded that their preparative methods resulted in a low-temperature Nb_2O_5 with a different structure (Allpress, Sanders & Wadsley, 1968).

$W_5Nb_{16}O_{55}$

The micrograph in Fig. 4 shows the image formed by the 001 reflexion of a crystal of $W_5Nb_{16}O_{55}$. The unfaulted region has a fringe spacing of 18·5 Å corresponding to a block width of five octahedra, but anomalies are clearly visible, *e.g.* at *A* and *B*. The spacing of the fringes at *A* and *B*, measured from microdensitometer traces such as that shown in Fig. 5(*a*) are 15 ± 1 Å and 22 ± 1 Å respectively. Spacings between shear planes, calculated from a model, are 14·8 Å for blocks of four octahedra, 18·8 Å for five, and 22·7 Å for six.

The basic structure of $W_5Nb_{16}O_{55}$ containing 4×5 octahedral blocks is, therefore, capable of being modified by the insertion at random of parallel slabs containing either 4×4 or 4×6 blocks. That this can be done is shown by the model in Fig. 5(*b*). The common width of four octahedra for all three sizes confines these non-periodic regions to the one direction, which as a result appear as planar 'defects'. The 4×4 blocks are the structural units of the phase $W_3Nb_{14}O_{44}$, but no compound with 4×6 blocks has yet been isolated. If it existed, its composition would be $W_7Nb_{18}O_{66}$.

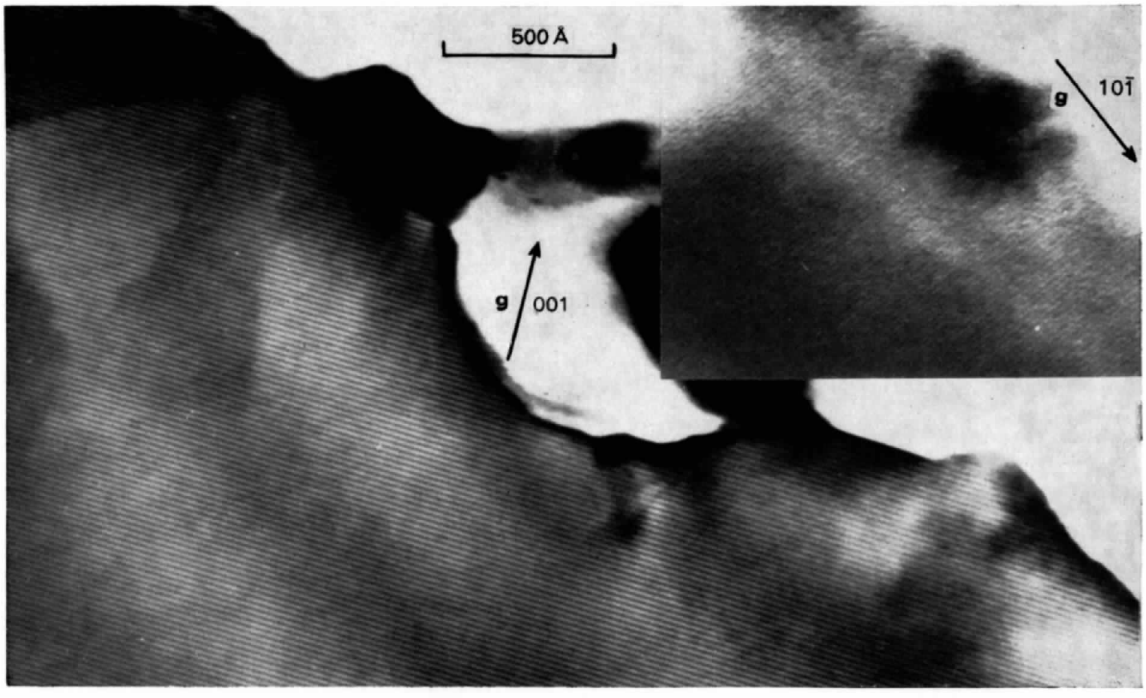

Fig. 3. Lattice image of part of a crystal of H–Nb_2O_5. The 001 fringe spacing is 16·8 Å. Inset: part of the same area tilted to reveal 10$\bar{1}$ fringes with a spacing of 17·7 Å.

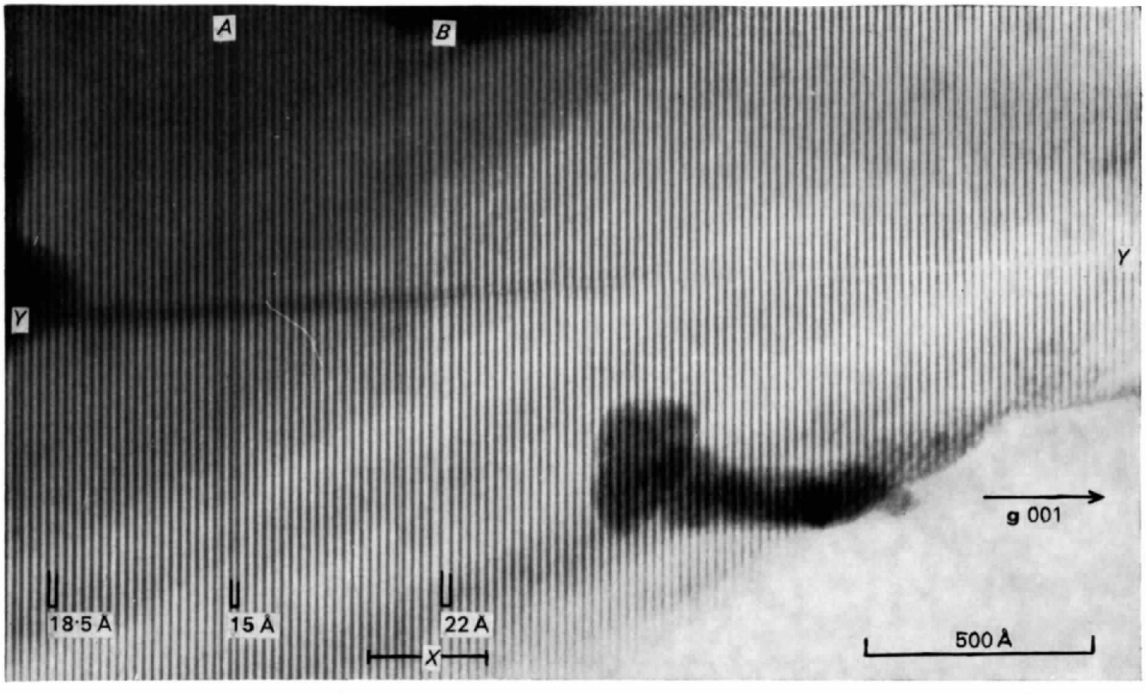

Fig. 4. Lattice image of $W_5Nb_{16}O_{55}$, formed using the ±001 reflexions. The normal fringe spacing of 18·5 Å is interrupted by faults, which at *A* are 15 Å and at *B* are 22 Å. *YY* is another fault, out of contrast in this orientation.

[*To face p.* 1159

$W_4Nb_{26}O_{77}$

If this simple model applies more generally, the intergrowth phase $W_4Nb_{26}O_{77}$ should be a rich source of structural faults, with the possibility of the regular alternating sequence of parallel slabs of 3×4 and 4×4 blocks degenerating into disordered regions.

In the perfectly ordered crystal (region *A* in Fig. 6), the image formed by the 00*l* reflexions ($l=\pm1, \pm2, \pm3$) consists of a double set of fringes. The microdensitometer trace across a micrograph of a typical region is shown in Fig. 7. It contains a regularly alternating sequence of large and small peaks. The peak-to-peak distance is constant at 13 Å $\left(=\frac{1}{2c^*}\right)$, but the valleys are spaced at 15 Å across the large peaks and at 11 Å across the small ones. Clearly, the large peaks correspond to blocks which are four octahedra wide (calculated spacing = 14·8 Å), and the small ones to blocks three wide (calculated spacing = 10·9 Å), while the valleys [or the black fringes in the micrograph in Fig. 6(*a*)] correspond to the shear planes. $W_4Nb_{26}O_{77}$ is the only ordered phase we have studied which has unevenly spaced shear planes [Fig. 1(*e*)], and the fact that a corresponding variation in fringe spacing appears in the micrograph confirms our belief that the image is produced by phase contrast.

Fig. 6(*b*) is the same area as Fig. 6(*a*), but with the crystal tilted slightly so that the image is formed with the ±200 reflexions. In this case, the fringes have a constant spacing of 15 Å, which is consistent with the fact that the shear planes in this direction separate blocks which are always four octahedra wide.

The faulted areas in Fig. 6(*a*) contain groups of fringes with constant rather than alternating spacings. The 11 Å group at *C* and the 15 Å fringes at *A* show the clustering of blocks of just the one size. These zones are, therefore, identifiable as the two phases $WNb_{12}O_{33}$ (block size 3×4) and $W_3Nb_{14}O_{44}$ (4×4) co-existing with $W_4Nb_{26}O_{77}$ (3×4 and 4×4) as microdomains in the one crystal fragment. A microdensitometer trace and a model of the probable structure of the faulted region marked *X* in Fig. 6 is shown in Fig. 8. The parallel set of lines drawn below the trace are collinear with one set of shear planes in the model, and they indicate the accuracy with which the spacings between valleys in the trace are reproduced in the model.

In Fig. 6(*b*), the faults which were resolved in Fig. 6(*a*) appear as diffuse vertical bands. The 15 Å fringes running almost perpendicular to these bands are slightly deviated as they cross them. This effect is qualitatively accounted for in the model in Fig. 8. The line *DD* is drawn parallel to the shear planes in this direction, and it deviates as it crosses each fault.

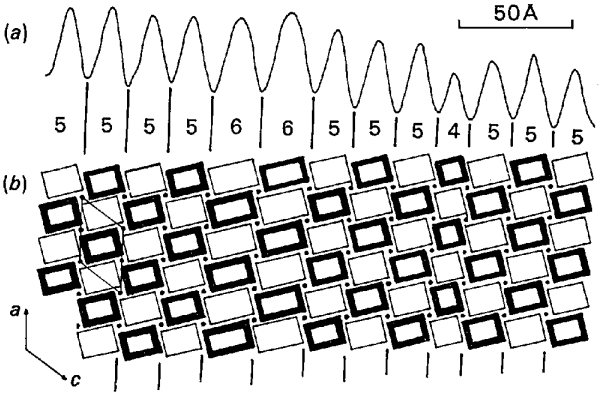

Fig. 5. (*a*) Microdensitometer trace of the faulted region marked *X* in Fig. 4. (*b*) Interpretation of the irregular spacings in terms of abnormally-sized blocks. The numbers refer to the width of each block in terms of octahedra. The shear planes are identified with the valleys in (*a*).

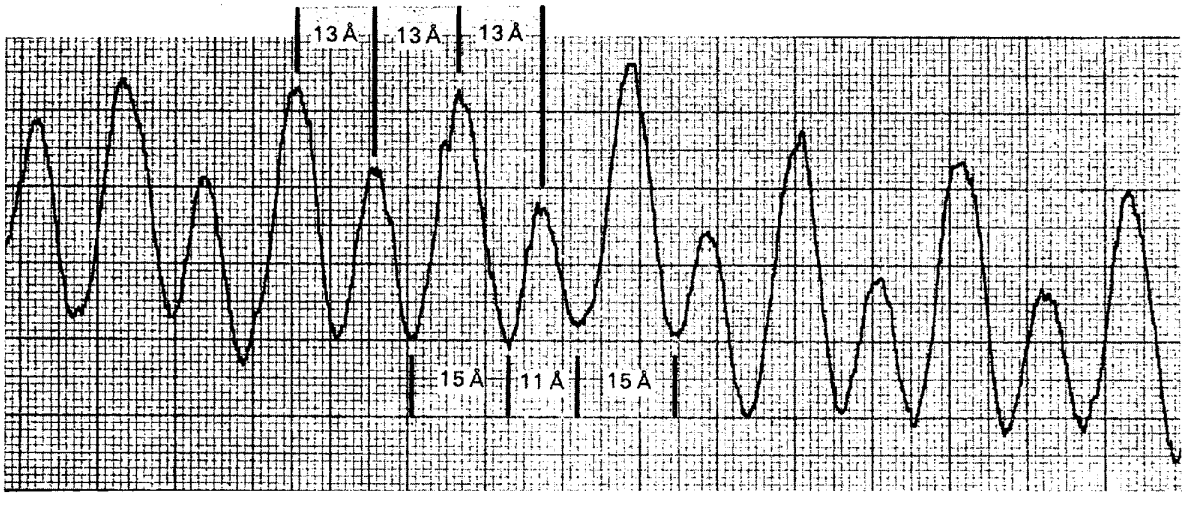

Fig. 7. Microdensitometer trace of a lattice image of a perfectly ordered region of $W_4Nb_{26}O_{77}$, similar to the region *B* in Fig. 6(*a*). The peaks are equidistant, but the valleys alternate between 11 Å and 15 Å corresponding to the two block units 3- and 4-octahedra wide.

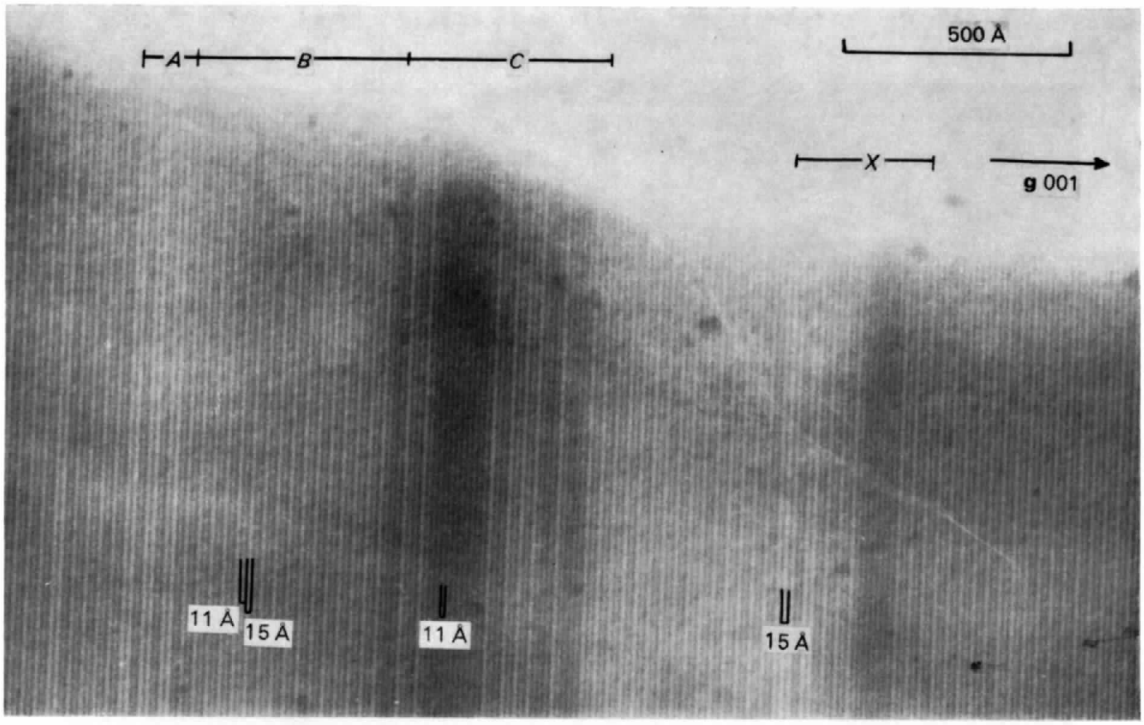

(*a*)

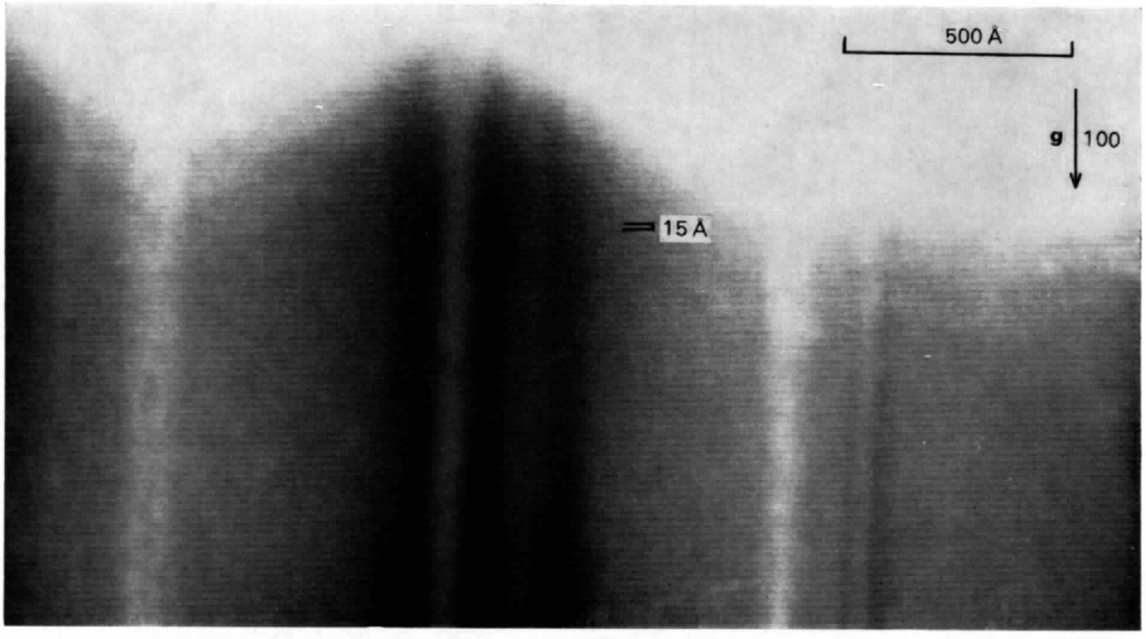

(*b*)

Fig. 6. Lattice images of $W_4Nb_{26}O_{77}$, the ordered intergrowth phase, using the $00l$ ($l = \pm 1, \pm 2, \pm 3$) [Fig. 6(*a*)] and ± 200 [Fig. 6(*b*)] reflexions. (*a*). The area *B* is the normal fringe structure. *A* is a different intergrowth region representing an abnormal block sequence. *C* is an even more disordered sequence containing a microdomain of $WNb_{12}O_{33}$. (*b*). The fringes have a constant spacing of 15 Å, despite the faults almost normal to them, which appear as diffuse bands. However, the fringes deviate slightly as they cross the fault bands.

[*To face p.* 1160

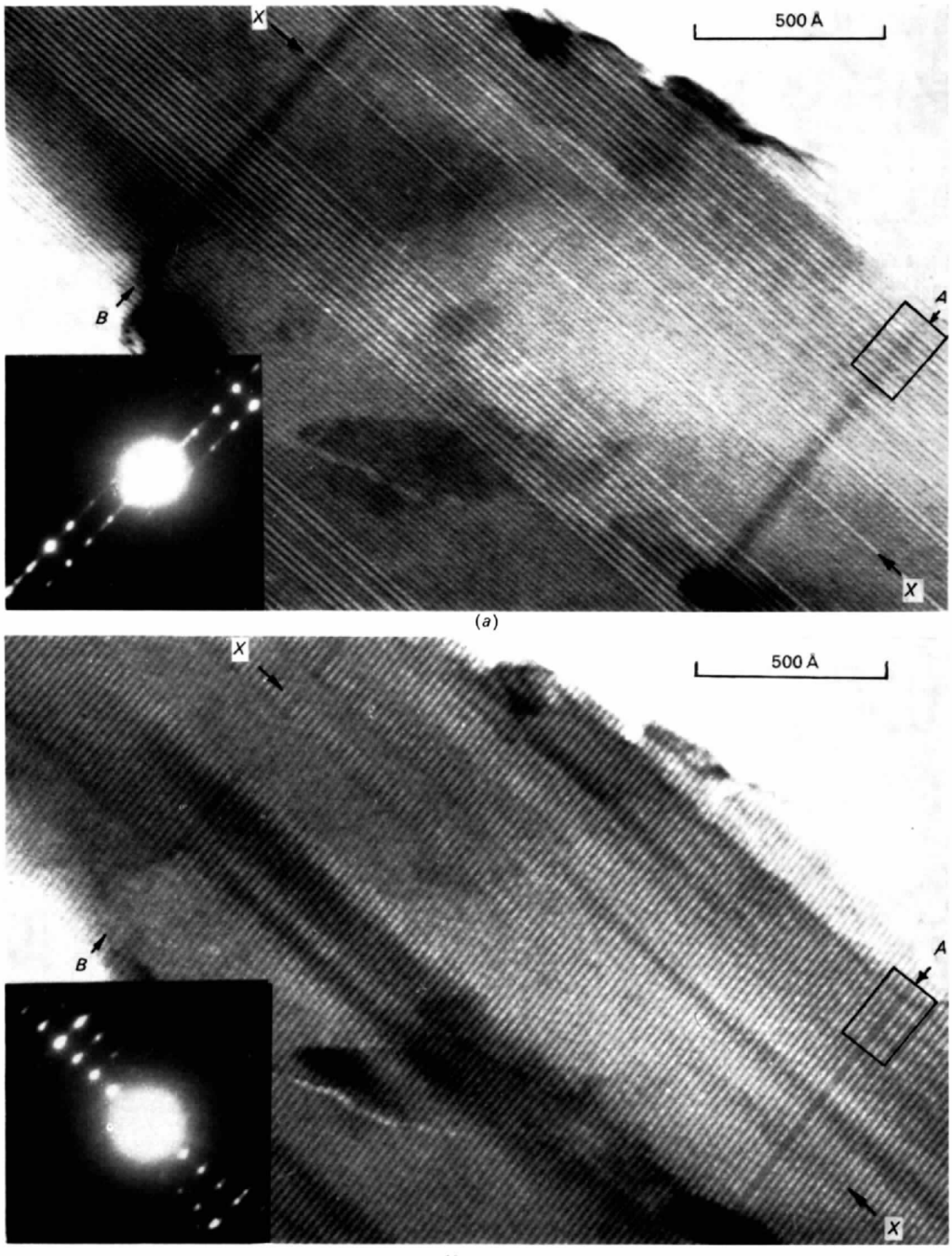

Fig. 9. Lattice image showing the random intergrowth of the two phases $W_8Nb_{18}O_{69}$ (blocks 5×5) and $W_5Nb_{16}O_{55}$ (blocks 4×5). The two sets of shear planes are imaged separately as black fringes in (*a*) and (*b*). The corresponding diffraction patterns are shown as insets. Most of the faults are parallel to *X*–*X* and the two marked *A* and *B* intersect these.

Intersecting faults

Intersecting planar faults have been found in some compounds, an example being given in Fig. 4(*a*), where one fault *YY* is out of contrast.

Fig. 9(*a*) and (*b*) are two views of the same area of a crystal of $W_8Nb_{18}O_{69}$ (blocks 5×5) imaged with the ±110 and $\pm1\bar{1}0$ reflexions respectively. Two sets of fringes with spacings of 18·5 Å and 15 Å in Fig. 9(*a*) show that there are two sizes of blocks, five and four octahedra wide, while the majority of the fringes in Fig. 9(*b*) have the period 18·5 Å. This portion of the crystal, therefore, contains domains of $W_5Nb_{16}O_{55}$ (blocks 4×5) intergrown with $W_8Nb_{18}O_{69}$.

In the orientation of Fig. 9(*a*), the faults *A* and *B* appear as diffuse bands, while the other set, parallel to *XX* are clearly visible. When the specimen was tilted into the orientation of Fig. 9(*b*), the faults parallel to *XX* were out of contrast and diffuse, whereas the faults at *A* and *B* were resolved as 15 Å blocks, four octahedra wide, in a region where the blocks were otherwise five wide.

A model for the small rectangular area in Fig. 9 is given in Fig. 10. Blocks four and five wide in the one direction intersecting blocks five and four in the other give four different units, 5×5, 5×4 and 4×5 (two orientations of the one size) as well as 4×4 where for this case the two abnormal fringes intersect. In this model the shear planes deviate slightly as they cross a fault normal to them, and this is also seen in the fringe pattern.

The micrograph of which Fig. 9 is a part showed two additional faults of 23 Å adjacent to each other and crossing the 15 Å and 18·5 Å fringes in another area. The intersections correspond to blocks 6×4 and 6×5 octahedra. Although the 6×4 blocks occurred as faults in Fig. 4(*a*) neither has been reported as the major component of a pure phase.

Fig. 11 shows another crystal of nominal composition $W_8Nb_{18}O_{69}$, tilted in order to image both sets of shear planes simultaneously. *A* is an area containing two orthogonal sets of 18·5 Å fringes and consists of $W_8Nb_{18}O_{69}$ (5×5 blocks); *B*, with 18·5 Å fringes in one direction and 15 Å fringes in the other is $W_5Nb_{16}O_{55}$ (4×5 blocks). This one area of a crystal, therefore, contains well-defined perfect regions of both phases side by side, together with faults *XX* traversing both of them. There is an obvious deviation of the fringes in the direction *XX* as they cross the boundary between the phases at *A* and *B*.

Terminated faults

Although in most cases the fault fringes traverse the entire field of the crystal which is transparent to electrons, there have been occasional examples of faults terminating within a crystal. The two micrographs in Fig. 12, taken from the same area of a crystal

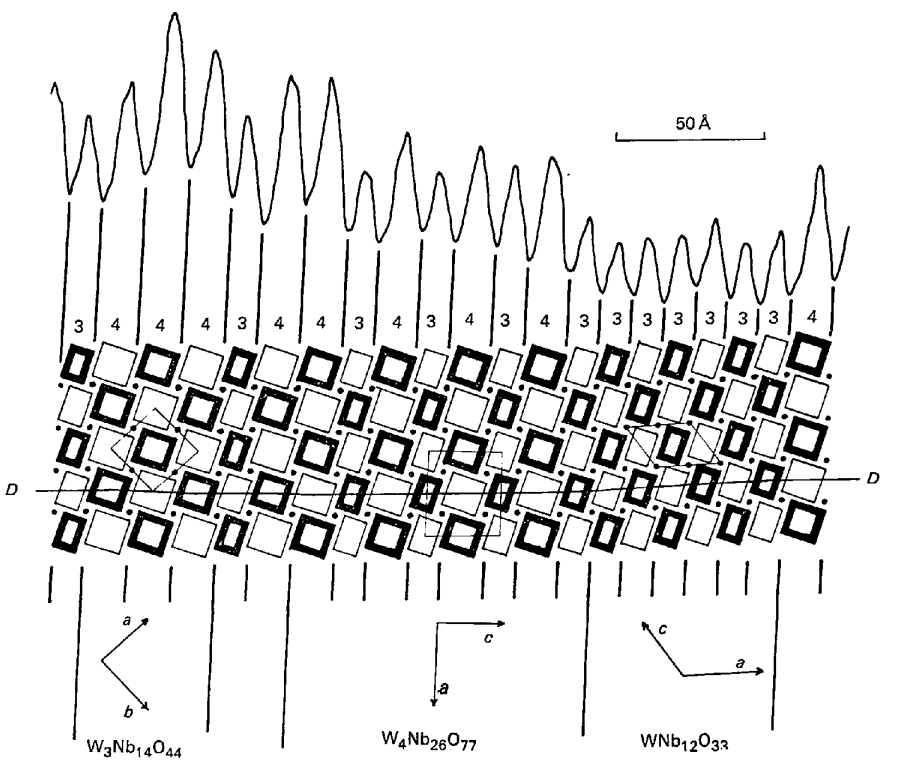

Fig. 8. Top: Microdensitometer trace of the region *X* in Fig. 6(*a*). Middle: Interpretation of this region in terms of the disordered intergrowth of 3×4 and 4×4 blocks. Microdomains of the three phases $W_3Nb_{14}O_{44}$, $W_4Nb_{26}O_{77}$ and $WNb_{12}O_{33}$ are identified (bottom).

of $W_5Nb_{16}O_{55}$ in different orientations, show several examples of this. The field in Fig. 12(*a*) consists of 15 Å fringes, except for the 18·5 Å fault fringes *BC*, *DE*, and *FG*, terminating at the ends of the faulted areas *AB* and *EF*, which are out of contrast in this image. In Fig. 12(*b*) the other set of fringes, mostly 18·5 Å, are in contrast and the faulted areas *AB* and *EF* contain 15 Å fringes, which change into 18·5 Å fringes as they cross the area *BE* and also below *F*. This means a reduction in the total number of fringes.

We have been able to propose a reasonable model for the simpler fault contained in the area *Y*, where the fringes *BC* and *XZ* are displaced at their point of intersection [Fig. 12(*a*) and (*b*)]. The block sizes may be deduced from the two sets of fringes, and the area *Y* has the block sequence:

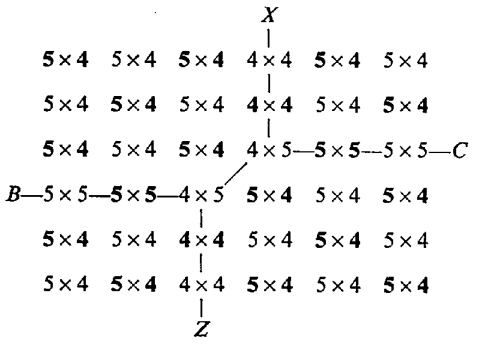

the two type-faces distinguishing the blocks at the two levels. Instead of intersecting as in the simple case illustrated by Fig. 10 the blocks constituting the faults are stepped as they cross. How this may be done is shown by the model in Fig. 13. The four at the centre are joined by octahedral edge-sharing and not by a tetrahedrally coordinated atom. This particular union has been demonstrated very recently by Andersson, Gruehn & Mertin (1968) for the polymorph M–Nb_2O_5 containing 4×4 blocks, and in the present case may be regarded as a single 'line defect' generating a fault with a 'dislocation'.

A model for the more complex terminations at *B*, *E*, and *F*, is not so readily devised. In the vicinity of *B* there are five 15 Å and one 18·5 Å fringes in the segment *AB* which are replaced by five 18·5 Å fringes in *BE*. The total number of octahedra, four for each 15 Å fringe and five for each 18·5 Å fringe must, therefore be the same on either side of the termination, even though there is a change in the number of fringes. This is clearly a different case from the simple intergrowth of two closely related phases, and can only be accounted for by octahedral edge-sharing by blocks within the plane of the paper as well as normal to it. Although this situation is covered by the structure of P–Nb_2O_5 (Petter & Laves, 1965), several interpretations of the structure of the fault are possible. We do not intend to give these until we have obtained more than this one example of these particular terminated faults, as an analysis of several of them should lead to a unique model.

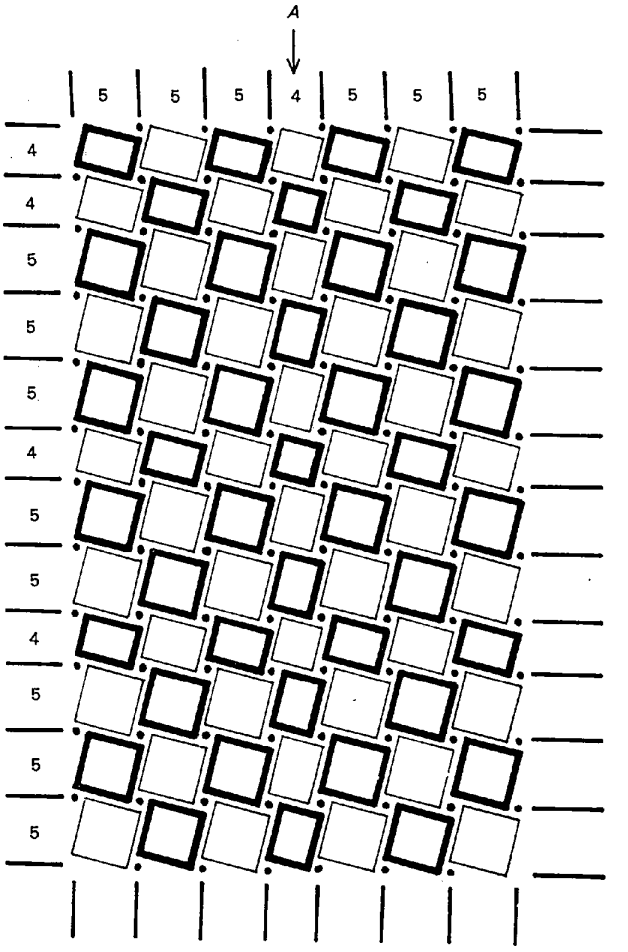

Fig. 10. Model of the rectangular area outlined near *A* in Fig. 9. The direction of the fault *A* is indicated.

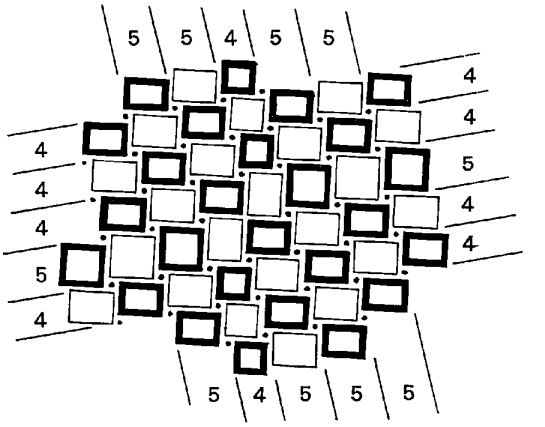

Fig. 13. Model which is consistent with the region *Y* in Fig. 12, showing displaced fringes. The numbers of octahedra in a block direction are given.

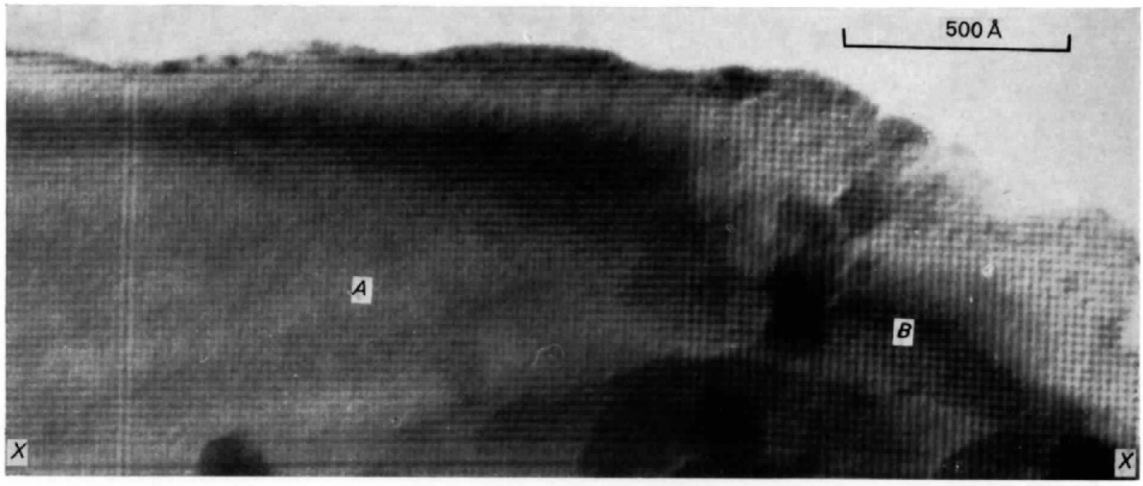

Fig. 11. Lattice image in which both sets of shear planes are revealed. *A* is a region of $W_5Nb_{16}O_{55}$, *B* is $W_8Nb_{18}O_{69}$. All the fringes parallel to *X*–*X* deviate at the boundary between *A* and *B*.

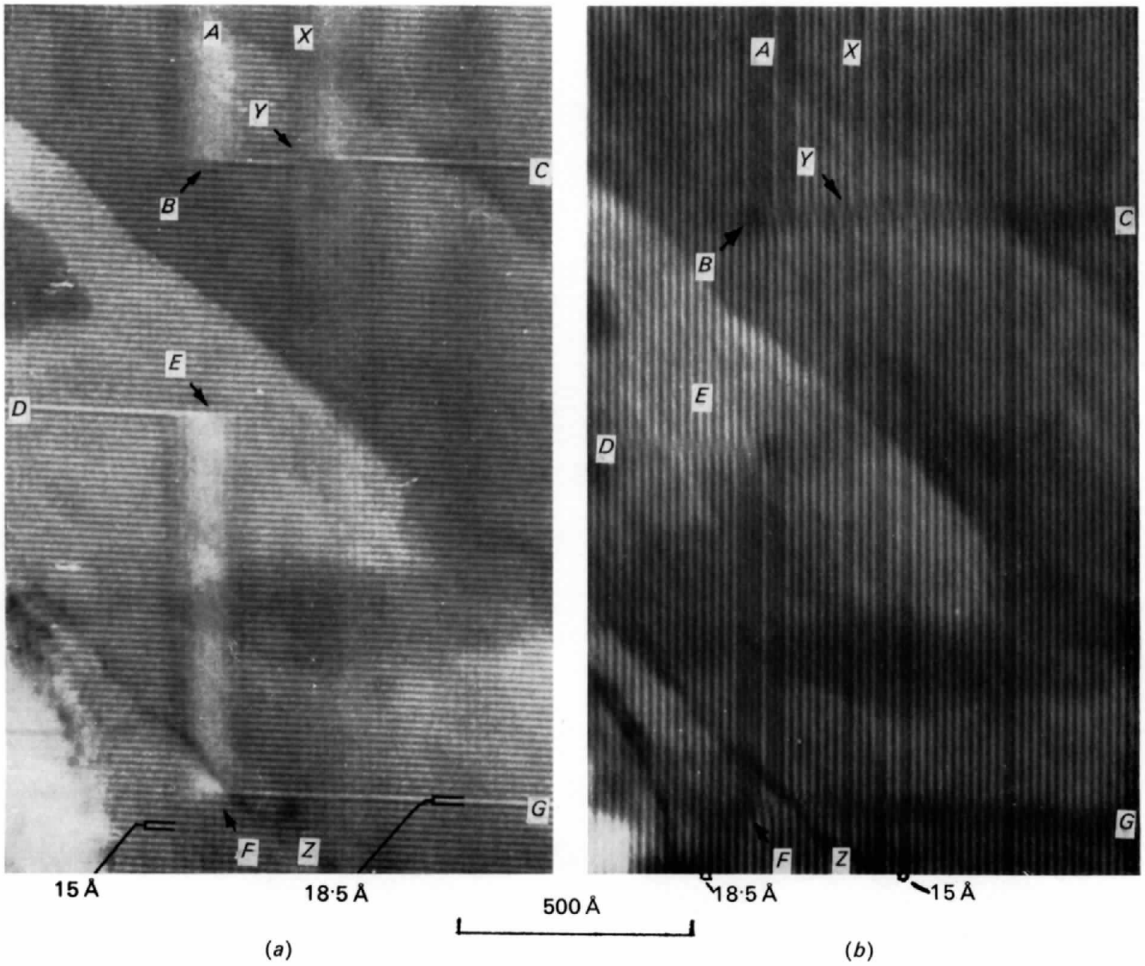

Fig. 12. Two lattice images of the same area of a crystal of $W_5Nb_{16}O_{55}$ showing faults terminating within the crystal at *B*, *E* and *F*, and displaced at *Y*. See text for reference to the other letters.

[*To face p.* 1162

Discussion

A phase prepared by reaction of two or more components in the solid state will have the composition of the starting mixture only if a number of experimental conditions are fulfilled. It is necessary to ensure that exactly weighed materials are thoroughly mixed, no component lost through preferential volatilization, an equilibrium state reached in the furnace, and the specimen cooled to room temperature without disproportionating. The composition of the mixed-oxide compounds in parts II, III and V was confirmed in these reports by crystal structure analyses, and although the Guinier powder pattern of each one was indexed on the basis of just the one phase, the present study shows that considerable local variation of structure is possible. This might well be a consequence of the necessarily selective way in which crystals are examined in the electron microscope. Only very thin fragments broken from larger crystals during grinding are sufficiently transparent to electrons, whereas the best-developed crystal, big enough to manipulate yet sufficiently small to minimize absorption, is carefully sought for an X-ray crystal structure analysis. There is no indication that the crystal perfection is disturbed by fracture.

Irregularities in the spacing of fringes in lattice images of the crystals we have studied can all be interpreted as being due to the insertion into one structure of fragments of another having a different stoichiometry. These fragments may be as small as a single sheet of octahedral blocks half a unit-cell thick, or a number of these sheets may be grouped together. Such an aggregation of faults of the one kind constitutes a microdomain of a second phase co-existing with the matrix. Faults differ from the matrix only by virtue of the block size in the direction approximately perpendicular to their boundaries. These boundaries are crystallographic shear planes, and their structure is identical with all other shear planes in the matrix which are parallel to them.

Slight changes in the overall stoichiometry of the crystal result from the presence of the faulted regions, because their composition is different from that of the matrix. A simple calculation illustrates this for Fig. 4. Ignoring the out-of-contrast fault *YY*, there are about 125 normal 18·5 Å fringes corresponding to $W_5Nb_{16}O_{55}$, four of 15 Å characteristic of $W_3Nb_{14}O_{44}$, and two of 22 Å due to the 6×4 blocks of '$W_7Nb_{18}O_{66}$'. The average composition of the region shown in the micrograph is, therefore,

$$125(W_5Nb_{16}O_{55})+4(W_3Nb_{14}O_{44})+2(W_7Nb_{18}O_{66}),$$

giving a fractional formula $MO_{2\cdot6187}$ which may be compared with $MO_{2\cdot6190}$ for fault-free $W_5Nb_{16}O_{55}$. The effects of two 22 Å faults are cancelled by two 15 Å faults, and the same change of composition would have been reached by inserting only two 15 Å faults consisting of 4×4 blocks in the matrix of 4×5 blocks.

Isolated faults, such as those in Fig. 4, will not affect the Bragg reflexions in an X-ray diffraction pattern. The homogeneity range of a phase as determined by X-rays will depend both upon the number of faults distributed in a random manner, and upon the sizes of groups of faults which can exist without being detected as a separate phase. The limits of detection are greatly extended by electron optical methods when the solid behaves as a phase grating. Lattice images contain information at the unit-cell level, and we have been able to observe and analyse faults as small as half a unit cell wide, represented by a single fringe, or even smaller regions for the special cases where fringes cross or terminate.

The structure of a host compound is virtually undisturbed by the presence of faults, and its lattice parameters will be unaffected by a range of chemical composition, a fact noted elsewhere in this series of articles, and for which a mechanism the same as the present one was suggested but without any direct evidence (Andersson, Mumme & Wadsley, 1966). This is a potentially useful diagnostic, and could be used in conjunction with chemical evidence to distinguish non-stoichiometry as a physical consequence of intergrowth from some other mechanism which changes the dimensions of the unit cell.

It might still be possible for other types of defect to be present in these compounds. Variation in the composition of a solid has usually been unquestioningly attributed to vacancies or interstitials. The concept of very wide ranges of homogeneity in a number of oxide systems, including the one studied here in parts I–VI, has often had to be rejected following the detection of closely-spaced and closely-related phases within the same composition limits. This is a consequence of a more critical experimental approach. Very small ranges of non-stoichiometry in the mixed niobium tungsten oxides, and possibly in all other families of shear structures as well, can now be attributed to the presence of planar faulted regions, which are non-periodic shear planes representing the partial intergrowth of one phase with another. Vacancies and interstitials are a necessary transient when one of these phases is forming, and play an important part in the movement of shear planes by a cooperative mechanism that has been proposed in outline (Andersson & Wadsley, 1966). This is being examined in detail, and will be reported elsewhere in due course (Wadsley & Andersson, 1969).

References

ALLPRESS, J. G., SANDERS, J. V. & WADSLEY, A. D. (1968). *Phys. stat. sol.* **25**, 541.

ANDERSSON, S. (1965). *Acta Chem. Scand.* **19**, 1401.

ANDERSSON, S., GRUEHN, R. & MERTIN, W. (1968). To be published.

ANDERSSON, S., MUMME, W. G. & WADSLEY, A. D. (1966). *Acta Cryst.* **21**, 802.

ANDERSSON, S. & WADSLEY, A. D. (1966). *Nature Lond.* **211**, 581.

COWLEY, J. M. & MOODIE, A. F. (1960). *Proc. Phys. Soc.* **76**, 382.
GATEHOUSE, B. M. & WADSLEY, A. D. (1964). *Acta Cryst.* **17**, 1545.
GRUEHN, R. (1965). *Mh. Chem.* **96**, 1789.
GRUEHN, R. (1967). *Naturwissenschaften*, **54**, 645.
GRUEHN, R. & SCHAFER, H. (1965). *J. Less-Common Met.* **10**, 152.
GRUEHN, R. & NORIN, R. (1967). *Z. anorg. allgem. Chem.* **355**, 176.
HASHIMOTO, H., MANNAMI, M. & NAIKI, T. (1961). *Phil. Trans. Roy. Soc.* **253**, 459.
HEIDENREICH, R. D. (1964). *Fundamentals of Transmission Electron Microscopy*, p.141. New York: John Wiley.
HEIDENREICH, R. D. (1966). *Proceedings of the 6th International Conference for Electron Microscopy*, **1**, 7.
PETTER, W. & LAVES, F. (1965). *Naturwissenschaften*, **52**, 617.
ROTH, R. S. & WADSLEY, A. D. (1965*a*). *Acta Cryst.* **19**, 26.
ROTH, R. S. & WADSLEY, A. D. (1965*b*). *Acta Cryst.* **19**, 32.
ROTH, R. S. & WADSLEY, A. D. (1965*c*). *Acta Cryst.* **19**, 38.
ROTH, R. S. & WADSLEY, A. D. (1965*d*). *Acta Cryst.* **19**, 42.
ROTH, R. S., WADSLEY, A. D. & GATEHOUSE, B. M. (1964). *Naturwissenschaften*, **51**, 262.
ROTH, R. S. & WARING, J. L. (1966). *J. Res. nat. Bur. Stand.* A**70**, 281.
SPYRIDELIS, J., DELAVIGNETTE, P. & AMELINCKX, S. (1967). *Phys. stat. sol.* **19**, 683.
WADSLEY, A. D. (1964). In *Non-Stoichiometric Compounds* Ed. L. MANDELCORN, p.98. New York: Academic Press.
WADSLEY, A. D. & ANDERSSON, S. (1969). In *Perspectives in Structural Chemistry*. Vol.III. Ed. J.D. DUNITZ & J.A. IBERS. New York: John Wiley. In preparation.

Acta Cryst. (1969). B**25**, 1164

The Crystal Structure of Cu_2CdGeS_4 and Other Quaternary Normal Tetrahedral Structure Compounds

BY E. PARTHÉ, K. YVON AND R. H. DEITCH*

School of Metallurgy and Materials Science, and Laboratory for Research on the Structure of Matter, University of Pennsylvania, Philadelphia, Pennsylvania, U.S.A.

(*Received* 19 *June* 1968)

Single crystal diffraction methods have been used to solve the crystal structure of Cu_2CdGeS_4: space group $Pmn2_1$ (C_{2v}^7); $a=7{\cdot}692$, $b=6{\cdot}555$, $c=6{\cdot}299$ Å. 4 Cu in 4(*b*): 0·252, 0·324, 0; 2 Cd in 2(*a*): 0, 0·848, 0·995; 2 Ge in 2(*a*): 0, 0·179, 0·490; 4 S in 4(*b*): 0·226, 0·344, 0·359; 2 S in 2(*a*): 0, 0·199, 0·838; 2 S in 2(*a*): 0, 0·851, 0·394. The Cu_2CdGeS_4 structure is a superstructure of wurtzite with $a\sim 2a_W$, $b\sim a_W\sqrt{3}$ and $c\sim c_W$. It presents the wurtzite analog to the stannite structure.

Five other compounds of general composition 1_2246_4 also show superstructures either of wurtzite or of sphalerite, while the twenty investigated 12_236_4 compounds have no ordered cation arrangement producing simple wurtzite or zincblende diffraction patterns.

The problems in the determination of quaternary zincblende or wurtzite related superstructures in general are discussed.

Introduction

The tetrahedral structures have recently been thoroughly reviewed and systematized (Parthé, 1963, 1964). One subdivision of these structures is the group of normal tetrahedral structures where every atom has four nearest neighbor atoms located approximately at the corners of a surrounding tetrahedron. There are two basic normal tetrahedral structures for elements; one is the normal cubic diamond structure, the other the structure of hexagonal diamond called also lonsdaleite (Bundy & Kasper, 1967; Frondel & Marvin, 1967). The binary, ternary or quaternary normal tetrahedral structure compounds have structures which are closely related to either cubic or hexagonal diamond. The structure types for these compounds are shown in Fig. 1. Binary equiatomic compounds select either the sphalerite (=zincblende) type related to cubic diamond or the wurtzite type related to lonsdaleite or a stacking variation of these. The ternary compounds have zincblende or wurtzite supercells with an ordered cation arrangement on the former Zn sites. The zincblende related types are the chalcopyrite ($CuFe^{III}S_2$) type and the famatinite (Cu_3SbS_4) type. A wurtzite analog to chalcopyrite was first found in β-$NaFeO_2$ by Bertaut & Blum (1954) and Bertaut, Delapalme & Bassi (1964). The structure of $BeSiN_2$ (Eckerlin, 1967) is essentially isotypic to β-$NaFeO_2$ except that $BeSiN_2$ has axial ratios much closer to the ones expected from the structural relationship to wurtzite. The enargite (Cu_3AsS_4) type is the wurtzite analog to the famatinite type. An ordered structure type for quaternary normal tetrahedral structure compounds is the stannite ($Cu_2Fe^{II}SnS_4$) type which is a superstructure type based on zincblende. When we started our research program no wurtzite

* Present address: General Telephone and Electronics Laboratories, Inc., Bayside, New York, U.S.A.